RADIATION FROM THE NONEQUILIBRIUM SHOCK FRONT

J. D. Teare,[1] S. Georgiev[2] and R. A. Allen[3]

Avco-Everett Research Laboratory, Everett, Massachusetts

ABSTRACT

Radiative heating of hypersonic objects becomes a significant contributor to the overall heat transfer at re-entry velocities in excess of 25,000 fps. The radiation from the equilibrium gas cap behind the bow shock wave is in general the major contributor to this heating, but appreciable "luminous front" radiation is also associated with the non-equilibrium region immediately behind strong normal shock waves. The present paper provides a brief review of the published information on radiative heating at 25,000 fps. In addition, the problem of calculating the radiation from the nonequilibrium region at higher velocities is discussed, and some recent experimental measurements for two molecular band systems are presented. Finally, the expected intensity level of nonequilibrium radiation at 35,000 fps is compared with the stagnation point heating caused by radiation from the equilibrium gas and by laminar aerodynamic heat transfer.

INTRODUCTION

During the past several years the heat transfer for re-entry velocities of up to 25,000 fps has been thoroughly explored. The stagnation point heating in particular has been investigated extensively (Refs. 1 to 4) both theoretically and experimentally.

Presented at ARS International Hypersonics Conference, Cambridge, Massachusetts; this work was supported by Electronics Research Directorate, Air Force Cambridge Research Laboratories, Office of Aerospace Research, United States Air Force, under Contract no. AF 19(604)-7458.

[1]Principal Research Scientist.

[2]Associate Scientist; presently Section Chief, Physics Dept. Research and Advanced Development Division, Avco Corporation, Wilmington, Mass.

[3]Senior Scientist.

Because of the strong normal shock associated with the stagnation point region of blunt re-entry bodies, the equilibrium air temperatures in that region can be of the order of 8,000 K and the nonequilibrium air temperatures in the shock front can be of the order of 25,000 K at satellite re-entry velocities. Thus there is appreciable thermal radiation from the shock heated air, and it has been shown (Ref. 5) that the "luminous front" radiation from the nonequilibrium region behind a normal shock can become more important than the equilibrium radiation at altitudes above about 150,000 ft. However, the total radiation heating has been found to be small compared with the aerodynamic heat flux for most flight situations involving re-entry velocities up to 25,000 fps.

For velocities in the neighborhood of 35,000 fps many of the feasible flight paths are such that the radiative heat flux to a re-entry body will be comparable with the aerodynamic heat flux. It thus becomes important to establish the level of any nonequilibrium radiation heating. At velocities in the range 30,000 - 40,000 fps the translational temperature close to the shock front is in the range 40,000 - 75,000 K. This temperature is reduced by the chemical and vibrational excitation processes occurring in the relaxation region behind the shock front. The radiation from this relaxation region shows a considerable overshoot of intensity above the equilibrium level, since it is associated with the high nonequilibrium temperature. This is shown schematically in Fig. 1. Only the translational and rotational degrees of freedom are excited in the air immediately behind the shock front, and the temperature T_i is given by the Rankine-Hygoniot relationships for $\gamma = 7/5$. For a flight Mach number M , the authors obtain

$$T_i/T_\infty = (35 - 5/M^2)(1 + 0.2M^2)/36$$

and T_i is much greater than the equilibrium stagnation temperature T_{eq} . Almost all of the chemical and excitation processes occurring in the nonequilibrium region are binary, so that the intensity of radiation from the region is proportional to the particle density, and the thickness of the region is inversely proportional to the density. Consequently, the integrated radiation flux emitted from the nonequilibrium region is independent of the particle density so long as the binary mechanisms predominate.

Any attempt to predict the nonequilibrium radiation profile must rely on calculations of the temperature, density and particle concentration histories behind the shock front. Such calculations can be made for moderate shock velocities, by

integration of the chemical rate equations (Refs. 6 to 9) with a given set of rate constants. The relevant rate constants are reasonably well determined (Ref. 10) for temperatures up to 8,000 K. However, in order to make calculations for a shock speed of 40,000 fps it is necessary to extrapolate an assumed temperature dependence for these rate constants to a temperature of 75,000 K. Preliminary calculations based on one such extrapolation indicate that the rate of radiation of energy from the nonequilibrium region could be an appreciable fraction of the flux of energy $\left(\frac{1}{2}\right)\rho V^3$ in the incident gas. Under such conditions the emitted radiation would contribute to the reduction of translational temperature, and must be included in the energy balance. Thus, at sufficiently low density the integrated radiation will depend on the flow energy which in turn depends on the density.

Two other effects can contribute to a reduction of the integrated nonequilibrium radiation under conditions of low density. First, the emitted radiation at low densities is reduced by "collision limiting," which occurs when the particle density is so low that there are insufficient collisions to maintain the population of excited states against the drainage by radiation. Second, truncation of the radiation profile occurs when the length of the relaxation region becomes comparable with the shock standoff distance.

The present paper provides a brief review of the published information on radiative heating at 25,000 fps. In addition, the problem of calculating the radiation from the nonequilibrium region at higher velocities is discussed, and some recent experimental measurements for two molecular band systems are presented. Finally, the expected intensity level of nonequilibrium radiation at 35,000 fps is compared with the stagnation point heating caused by radiation from the equilibrium gas and by laminar aerodynamic heat transfer.

RADIATIVE HEATING AT 25,000 FPS

The relative magnitudes of the radiative and convective heat transfer at the stagnation point are shown in Fig. 2, for a flight velocity of 25,000 fps. Apart from a change of nose radius, the information presented is identical with that given in Ref. 5. At this velocity the stagnation temperature decreases slightly with increasing altitude; the black body radiation (in w/cm^2) corresponding to this stagnation temperature is thus a known function of altitude, as plotted. The equilibrium radiation intensity, $\bar{I}w/cm^3$-ster, is a known function

(Ref. 3) of stagnation temperature and density, and is thus also a known function of altitude for a given velocity. For a blunt body and an optically thin gas, the radiative flux towards the stagnation point is $2\pi\bar{I}$ w/cm^2 per cm thickness of hot gas. In the present case, for which the nose radius is specified as 10 ft, we may multiply $2\pi\bar{I}$ by a gas cap thickness of $\sim$30 cm, to obtain the plotted values of I (in w/cm^2). Observe that these values of I , which vary approximately as $\rho^{1.7}$, exceed the black body radiation intensity when $\rho/\rho_o \gtrsim 3 \times 10^{-2}$. This merely means that the 30 cm gas cap thickness is no longer optically thin; when I exceeds about 10% of the black body value, it is necessary to take account of re-absorption in the gas (Ref. 11). At very high densities the equilibrium radiation intensity is given by the black body limit.

The total radiative flux to a stagnation point is obtained by adding the integrated nonequilibrium radiation to the equilibrium flux obtained as described. The detailed spectral measurements (Ref. 5) carried out at 23,000 fps indicate that the integrated luminous front intensity at 25,000 fps is not greater than 10 w/cm^2, as shown in Fig. 2. Thus the luminous front flux is comparable with or greater than the equilibrium flux for $\rho/\rho_o \lesssim 10^{-3}$. For a body of infinite size and with infinite excitation rates, the high altitude radiative flux would not fall below a "plateau" at the 10 w/cm^2 level. In practice, a fall-off is to be expected, due partly to "collision limiting," which vitiates the binary scaling near the shock front, and partly to truncation of the nonequilibrium region caused by the finite standoff distance for a normal re-entry body. Collision limiting for a large body would cause the integrated intensity to vary linearly with ρ , whereas severe truncation of a binary region introduces a ρ^2 dependence. This may be seen from Fig. 3 if one assumes a linear rise of radiation intensity behind the shock front. Doubling the density then quadruples the integrated flux for a given truncation distance.

The laminar aerodynamic heat transfer rate (Ref. 2) as a function of ambient density is also plotted on Fig. 2. It is seen that, even for the large nose radius chosen, the aerodynamic heating is approximately an order of magnitude larger than the radiative flux at altitudes above about 150,000 ft. The aerodynamic heat transfer rate varies inversely with the square root of the nose radius, whereas the equilibrium radiative flux depends on the thickness of the gas cap,[4] and varies linearly with nose radius. Thus, the relative positions of the equilibrium radiation and aerodynamic heat transfer curves can be shifted by variation of the nose radius. The position of the luminous front plateau, however, is independent of the nose radius. The approximate limits (Ref. 13) of free molecule

flow and of the disappearance of the inviscid shock layer for a nose radius of 10 ft are also indicated on Fig. 2.

RADIATION CALCULATIONS

Equilibrium Radiation

Under equilibrium conditions, most of the radiation from air at temperatures above 5,000 K arises from various molecular band systems or from Kramers radiation. In the present discussion, attention will be confined to the former, since these are more susceptible to significant overshoot in the nonequilibrium region behind the shock front.

The radiation intensity for a given molecular band system is proportional to the excited state population. In general, the latter may be related directly to the ground state population by means of a Boltzmann factor. Thus

$$[A^*]/[A] \propto \exp(-E/T_e) \tag{1}$$

where E is an activation energy, and T_e is a temperature which characterizes the electronic excitation of the molecule A. For example, for the N_2 first and second positive band systems and for the N_2^+ first negative system, the total radiation may be approximated by the formulas

$$N_2(1+)\ \bar{I}_a = 2.5 \times 10^{-13}[N_2]\exp(-90{,}000/T_e)\ \text{w/cm}^3\text{-steradian} \tag{2}$$

$$N_2(2+)\ \bar{I}_b = 3.4 \times 10^{-11}[N_2]\exp(-129{,}500/T_e)\ \text{w/cm}^3\text{-steradian} \tag{3}$$

---

[4] This is true only if the total rate of energy loss by radiation from the gas is small compared with the incident energy flux $\left(\frac{1}{2}\right)\rho V^3$. If the radiation is sufficient to cause appreciable cooling of the gas in the stagnation region, then $\bar{I}$ will vary drastically with distance s behind the shock (Ref. 12). The radiative heating is then obtained by evaluating

$$\int_0^S 2\pi \bar{I}(s)\, ds$$

where S is the thickness of the gas cap.

$$N_2^+(1-)\,\bar{I}_c = 0.9 \times 10^{-12}\,[N_2^+]\exp(-36{,}000/T_e)\ \text{w/cm}^3\text{-steradian} \qquad (4)$$

Here $[N_2]$ is the number of ground state nitrogen molecules per unit volume, and $[N_2^+]$ is the number of ground state molecular ions per unit volume. At thermodynamic equilibrium, T_e will be equal to the translational temperature, and Eqs. 2, 3 and 4 become identical[5] with the expressions quoted in Ref. 14. The numerical constants were chosen to provide agreement with experiments (Ref. 15).

For an optically thin gas, the contributions of the individual band systems to the radiative heating at the stagnation point may be obtained by evaluating $\int_0^S 2\pi \bar{I}_j$ over the thickness S of the equilibrium gas cap. Summing the contributions (including Kramers) obtained in this manner leads to a total equilibrium radiation identical with that discussed in the previous section.

Close to the shock front, as has been pointed out, the translational temperature can be an order of magnitude higher than the equilibrium temperature appropriate to a given shock speed. If T_e becomes comparable with the translational temperature when the latter is still substantially higher than the equilibrium temperature, it is clear that band systems with high activation energies as above can exhibit radiation overshoots. However, not all molecular band systems with high activation energies exhibit an overshoot. For example, the Schumann-Runge radiation behind a shock front in pure oxygen does not overshoot (Ref. 19), and it may be deduced (Ref. 20) that the population of the excited state $B^3\Sigma$ is coupled to the O atom population as well as to the ground state O_2 population, thus inhibiting the over-population of the $B^3\Sigma$ state.

Upper Bound Estimates of Nonequilibrium Radiation From Molecular Band Systems

Various numerical investigations have been made of the physical quantities in the nonequilibrium region behind strong normal shock waves in air and its component gases. Models have

[5] With the exception that a reduction in f number for the N_2^+ (1-) system (Ref. 16) has been incorporated into Eq. 4. A revised f number (Ref. 17) for the N_2 (1+) system has recently been quoted by Treanor (Ref. 18), but the change has not been included in Eq. 2.

been set up (Refs. 6 to 9) which describe the chemical and excitation processes occurring in the shock heated gas. For a given choice of rate constants, profiles of the temperature, density and particle concentrations in the relaxation region are obtained by integrating the appropriate rate equations subject to constraints imposed by the conservation requirements.

Figure 4 shows the calculated temperature (Ref. 5) and particle concentration histories behind a normal shock travelling at 23,500 fps into air at an initial pressure of 20μ Hg, equivalent to an altitude of 255,000 ft. The atom concentrations build up from zero, and the translational temperature drops rapidly from 25,000 K. The substantial overshoot of NO concentration and the slight overshoot of ionization fraction are characteristic of shock velocities in this range. Associated with the electron profile (but not illustrated) is the corresponding history of N_2^+ concentration. The bottom curve shows an upper bound estimate of the radiation from the N_2^+ first negative band system, obtained by assuming the population of the $B^2\Sigma$ state of the N_2^+ to be in equilibrium with the ground state ($X^2\Sigma$). The plotted radiation intensity at a given distance behind the shock front is obtained by insertion of the local translational temperature and N_2^+ concentration into Eq. 4. In practice the tail end of this radiation estimate is probably accurate, since T_e will ultimately become equal to the translational temperature, but closer to the shock front the method overestimates the intensity, since the excitation processes will require a finite time to populate the $B^2\Sigma$ state.

The intensity estimate given exhibits a finite rise time, since the ground state N_2^+ concentration must build up from zero. A more refined estimate may be made by consideration of some excitation mechanism, but the method described gives a reasonable upper bound for the radiation intensity for this band system. The same technique cannot be used to estimate the radiation from the N_2 first and second positive band systems, since these have no built-in rise times. It is clear that large overshoots for these band systems are to be expected if Eqs. 2 and 3 are valid. For example, if $T_{eq} = 6{,}000$ K and if T_e is equal to the translational temperature over the range $T_{eq} + 1000 > T \geq T_{eq}$, then $\exp(-90{,}000/T_e)$ decreases by a factor of 8.5 as T_e decreases from 7,000 K to 6,000 K. Because of this steep temperature dependence, it is not reasonable to assume that T_e equals the translational temperature early in the relaxation history, since Eqs. 2 and 3 would then yield extremely high intensity predictions. Some consideration of the excitation times or mechanisms thus becomes essential.

In initial attempts to estimate the nonequilibrium radiation

intensity from these two band systems at 35,000 fps, recourse was made to lower velocity experiments carried out at Avco-Everett Research Laboratory. The experiments showed the expected overshoot of the N_2 first positive radiation, and provided measurements of the time to peak intensity. An extrapolated value of the distance to peak radiation d_m was used in the following manner. A radiation profile was assumed as in Fig. 5, based on a calculated profile of translational temperature, T . The radiation intensity was assumed to rise linearly up to a distance d_m behind the shock, at which point T_e was assumed equal to T . The subsequent decrease of radiation was controlled by the decay of T and of the N_2 ground state population. Estimates made in this manner are very sensitive both to the value of d_m and to the computed T history. The latter is itself dependent on the extrapolation of rate constants by means of an assumed temperature dependence, and on the mechanism of coupling between vibration and dissociation (Ref. 21).

Calculations based on some reasonable assumptions about the rate constants, and on extrapolation of experimental values of d_m , immediately uncover another problem. The total flow power per unit area of the bow shock is $\left(\frac{1}{2}\right)\rho V^3$, as shown in Fig. 6 for an altitude of 200,000 ft. The calculations can yield a rate of loss of energy by radiation comparable with or exceeding this $\left(\frac{1}{2}\right)\rho V^3$ limit. Thus, it becomes necessary to include the radiative power loss in the energy balance, as in the equation

$$\left(h_\infty + \frac{1}{2} V_\infty^2\right) - \left(h_x + \frac{1}{2} V_x^2\right) = \frac{10^7}{\rho_\infty V_\infty} \int_0^x 4\pi \bar{I}(s)\, ds \qquad (5)$$

where h_∞ and h_x denote the specific enthalpy in the unshocked gas and in the gas at distance x behind the shock front respectively. When coupled with the mass and momentum continuity relations

$$\rho_x V_x = \rho_\infty V_\infty$$

and

$$p_x + \rho_x V_x^2 = p_\infty + \rho_\infty V_\infty^2$$

respectively, Eq. 5 provides the constraints on the chemical behavior in the relaxing gas. The radiation integral must be evaluated from the shock front concurrently with integration of the chemical rate equations. It is assumed that the gas is transparent, so that absorption can be neglected. The radiation loss is evaluated over 4π steradians, this being twice the flux towards the stagnation point. Since in a binary situation the integral in Eq. 5 would be independent of density, this effect clearly becomes more important as the density is reduced, and it invalidates the binary scaling concept.

Figure 6 also shows the results of calculations of the integrated nonequilibrium radiation based on the "nonadiabatic" model described above. The calculations include only the radiation from the N_2 first and second positive band systems. With this particular set of assumptions, the radiation prediction is clearly extremely high from an engineering viewpoint. The range of uncertainty for the extrapolations is such that different choices of assumptions could reduce the predicted intensity by one or two orders of magnitude, or even move it closely to the $\left(\frac{1}{2}\right)\rho V^3$ limit. Collision limiting could be expected to reduce the intensity at the altitude chosen for Fig. 6, but the relevant cross sections have not yet been experimentally determined. Much remains to be learned about the chemical rates and excitation mechanisms before more accurate predictions can be made. The need to provide a more solid foundation for these predictions has motivated the current intensive experimental and theoretical research study of radiation behind high velocity shocks at the Avco-Everett Research Laboratory and elsewhere.

Collision Limiting

Collision limiting is a phenomenon frequently encountered in gas discharge work. In the context of the present problem it was discussed by Keck et al. (Ref. 15) with regard to the equilibrium radiation measurements in high temperature air. The radiation intensity is proportional to the excited state population, which is produced by bi-molecular collisions. When the density is sufficiently high there are sufficient collisions to maintain the excited state population in equilibrium with the ground state. Only a small proportion of the excited molecules are de-excited by emission of a photon. At lower densities, however, the number of collisions in unit time becomes comparable with the rate of radiative de-excitation. The excited state population then falls below the local equilibrium level which prevailed at high density. An analogy may be drawn by consideration of the filling of a pail which has a hole in it.

If a sufficient flow of water is directed into the pail, the water in the pail will reach a certain equilibrium level. If the flow into the pail is reduced, then this equilibrium level will be lowered.

For a simple system involving excitation and de-excitation of a species by collisions

$$A + B \underset{D}{\overset{E}{\rightleftarrows}} A^* + B$$

and de-excitation by emission of a photon

$$A^* \rightarrow A + h\nu$$

a rate equation may be written in the form

$$\frac{dA^*}{dt} = k_E \cdot B \cdot A - k_D \cdot B \cdot A^* - \frac{A^*}{\tau_R} \tag{6}$$

Here k_E and k_D are the rate constants for the excitation and de-excitation processes, and τ_R is the radiative lifetime appropriate to the excited state A^*. Under conditions where dA^*/dt is small compared with the dominant terms in Eq. 6, the excited state population takes up a steady state level

$$A^*_{ss} = \frac{A \cdot k_E/k_D}{1 + (k_D \cdot B \cdot \tau_R)^{-1}}$$

Near equilibrium, by the principle of detailed balancing

$$k_E/k_D = K(T)$$

similar in form to Eq. 1. Using a collision time τ_c defined by

$$k_D \cdot B = 1/\tau_c$$

the steady state number density may be written

$$A^*_{ss} = \frac{A \cdot K(T)}{1 + \tau_c/\tau_R}$$

Since the radiation intensity is proportional to A^*, the ratio τ_c/τ_R thus determines two distinct regimes of density dependence for the intensity. At high densities, $\tau_c << \tau_R$, and

$$A^*_{ss} = A^*_{eq} = A \cdot K(T)$$

Hence, the intensity is proportional to A, or to the first power of the ambient density. There are many collisions within a radiative lifetime, radiation drainage can be completely ignored and the process is binary. At the other extreme, for very low densities $r_c >> r_R$ and $A^*_{ss} = A \cdot K \cdot (T) \cdot r_R / r_c$, or the intensity is proportional to $k_D \cdot B \cdot A$, and thus to $k_D \rho^2$. The rate equation is then dominated by a unimolecular term, and binary scaling is invalidated. When r_c and r_R are of the same order of magnitude, the "local equilibrium" intensity is reduced by a factor $(1 + r_c / r_R)$.

The measurements of Keck and co-workers indicated that the de-excitation cross section for the O_2 Schumann-Runge radiation must be at least $10^{-15} cm^2$. If a cross section of this magnitude is appropriate to other band systems we should expect to see collision limiting effects at densities shown in Table 1.

Table 1[a] Densities below which radiation from various band systems is "collision limited" based on a de-excitation cross section of 10^{-15} cm^2.

Band System	Critical Density – ρ_o
O_2 Schumann-Runge	0.0055
NO γ	0.0009
NO β	0.0013
N_2 first positive	0.0010
N_2 second positive	0.031
N_2^+ first negative	0.036[b]

[a]Extracted from Ref. 15.
[b]Revised in accordance with f number quoted in Ref. 16.

Here the "critical" densities are determined as those which lead to $r_c \approx r_R$. So far collision limiting in the present context has not been observed experimentally, but it should be observable by means of existing equipment unless the cross section is much greater than 10^{-15} cm^2.

If the population mechanisms of the N_2 first and second

positive band systems are similar, one would expect a steeper temperature dependence for the second positive band system because of its higher activation energy. Although the second positive system is not a major contributor to the nonequilibrium radiation at velocities below 25,000 fps, it could play a bigger role at higher shock velocities. Indeed, for the model used in the predictions of Fig. 6, the second positive system does become dominant. However, the second positive system has the higher f number and should, therefore, be more susceptible to the collision limiting effect.

Estimation of Other Radiation

The principal contributions to the nonequilibrium radiation are expected to come from the three band systems discussed previously. Contributions may also be expected from those other band systems (Ref. 15) which are observed under equilibrium situations, including the NO β and γ bands and O_2 Schumann-Runge radiation. Kramers radiation, which is associated with the acceleration of capture of electrons by atoms and ions, also plays an increasing role in the equilibrium situation as the stagnation temperature is increased. The formulas (Ref. 14) for Kramers radiation are not characterized by strong Boltzmann factors as are those for the molecular band systems discussed, and any overshoot in intensity would be almost directly proportional to an overshoot of electron concentration. Preliminary calculations of ionization history behind shock waves at velocities up to 35,000 fps do not exhibit strong overshoots when electron impact phenomena are ignored. Reactions of the form

$$O + e \rightarrow O^+ + 2e$$

should assume increasing importance at the higher shock speeds, but estimates of this effect indicate that the electron concentration is unlikely to overshoot by more than a factor of two.

A complete understanding of the nonequilibrium radiation cannot be accomplished until measurements have been made over the entire wavelength region of interest. This region can be established by examination of integrated black body curves for the appropriate temperature range. Figure 7 shows integrals of the black body radiation from the far u.v. and from the far i.r. as a function of wavelength, for various temperatures. If it were possible for the relaxing gas to radiate as a black body at 50,000 K, and if one were interested in determining any spectral region in which the intensity exceeded, say, 10 w/cm^2, then the curves of Fig. 7 show that it would be necessary to survey the wavelength region from 125A to 160,000A.

At shock speeds which produce translational temperatures in excess of 50,000 K, there is thus a discouraging possibility of high intensity of radiation at wavelengths as small as 100A. The i.r. extreme of the region of interest is less sensitive to temperature, but both extremes merit careful experimental investigation.

Kivel (Ref. 5) showed how this black body estimate of the lower wavelength could be raised if one had a reasonable temperature history for the relaxation region, permitting an estimate of the number of collisions sufficiently energetic to produce u.v. radiation. Using temperature-distance information as in Fig. 4 one may evaluate the integral

$$I = \int_{h\nu}^{\infty} \left(\int_{0}^{L} \frac{N \cdot h\nu \, ds}{kT \tau_{c\nu}} \right) d\, h\nu \qquad (7)$$

where N is the particle density at distance s behind the shock, T is the corresponding temperature, and $1/\tau_{c\nu}$ is the frequency of collisions with sufficient energy to excite radiation at frequency ν. With an assumed cross section of 10^{-15} cm^2 and a mean particle speed of 3×10^5 cm/sec, so that

$$1/\tau_{c\nu} = 3 \times 10^{-10} \, N \exp(-h\nu/kT) \, sec^{-1}$$

the integral has been evaluated for the shock history of Fig. 4, to a distance L = 2 cm behind the shock front. Values of I as a function of wavelength are plotted on Fig. 7.

A similar theoretical check on this u.v. limit for a higher shock velocity could be made as soon as there is sufficient understanding of the chemistry to permit calculation of temperature histories consistent with radiation data obtained in the spectral regions accessible to measurement.

Shock Tube Radiation Studies

Shock tubes have been used in various research laboratories for radiation measurements, and have provided the main source of experimental information on radiation emitted by high temperature air. Most of the results previously reported (Ref. 15) by the Avco-Everett Research Laboratory have related to radiation from equilibrium air, oxygen and nitrogen, and have been obtained in conventional combustion-driven shock tubes of 1.5 in. or 6 in. diameter. Measurements of luminous front radiation from air (Ref. 5) and nitrogen (Ref. 22) have been reported.

Radiation experiments have also been carried out in the 24-in. diam shock tube described by Lin and Fyfe (Ref. 23), and recent work with an electrically-driven shock tube has yielded data on the luminous front in air at velocities up to 37,000 fps.

1. Apparatus and Experimental Procedure

Figure 8 shows a schematic diagram of the 1.5 in. shock tube, recording equipment and optical arrangement. The shock tube has a pyrex test section 15 ft long and of 1.5 in. inside diam. The high pressure driver section is separated from the low pressure test section by a steel diaphragm. The driver is of stainless steel, 3 ft in length and 1.5 in. inside diam. The test section is evacuated by an oil diffusion pump prior to introducing the test gas. Pressures of less than 2.0μ Hg and virtual leak rates of less than 1.0μ Hg per min are obtained. A flow system is used to minimize impurities due to outgassing of the apparatus, and the test gas is passed through a liquid nitrogen cold trap to remove water vapor. Initial pressure in the test section is measured by a manometer with an estimated maximum error of 0.4%.

The shock speeds are measured by observing with a single photomultiplier the radiation from the shock as it passes a series of six equally spaced slits arranged 10 in. apart along the latter half of the shock tube. The output of the photomultiplier is doubly differentiated and displayed on a folded oscilloscope sweep which is normally read to the nearest 0.4 μsec. A speed profile can be constructed and the velocity at the test section can be determined with a maximum error of about 1%.

Both photographic and photometric measuring techniques have been used in the shock tube experiments. In order to ascertain the origin of the radiation being studied, spectra of the shock heated air (Ref. 15) and nitrogen (Refs. 9 and 22) were taken using the race track techniques reported by Rosa (Ref. 24). It has been established that the impurity radiation is caused by CN and NH molecules, located mainly in the vicinity of the shock tube walls.

Photometric measurements have been made using a dual channel grating monochromator as shown in Fig. 8. The entrance slit of the monochromator is imaged perpendicular to the shock tube at the center of the test gas by an optical train consisting of two aluminized mirrors. The monochromator is equipped with three photomultipliers; two of these measure the radiation intensity in two adjacent narrow wavelength bands selected by the monochromator and the third monitors a fraction of the

radiation passing through the entrance slit. The outputs of the photomultipliers are fed directly to Tektronix 545 oscilloscopes equipped with 53K/54K preamplifiers.

The optical resolving time is determined by the entrance slit width, usually set at 0.50 mm. Therefore, for a shock speed of 5mm/μsec the optical resolution is approximately 0.1 μsec. The theoretical electronic rise time has been evaluated to be approximately 0.03 sec.

For studying the radiative relaxation overshoot of the N_2 first positive system in pure nitrogen, a Dumont K1292 photomultiplier has been used as the monitor with a filter placed directly in front of it to cut off radiation below 5500A. This arrangement monitors essentially only the $N_2(1+)$ system, and oscillograms taken of the overall radiation overshoot, equilibrium region and driver gas interface are shown in Fig. 9. For an initial shock tube pressure of 2mm Hg, oscillograms are shown for three different shock speeds. The radiation is observed to overshoot, then decay to an equilibrium value within a few microseconds.

The approximate range of velocity and density for which equilibrium or luminous front radiation measurements have been made in conventional shock tubes is shown by the crosshatched area **A** in Fig. 10. The 24 in. diam shock tube permits operation at 20μ Hg, extending the range accessible to luminous front experiments as shown by the area B. The contours plotted on Fig. 10 show the equilibrium radiation flux[3] to the stagnation point ($2\pi\bar{I}$ in the notation of the second section) as a function of flight velocity and altitude.

Recent experiments have been carried out in an electrically driven shock tube developed by Camm. The approximate velocity-density region accessible to this device is shown by the area C in Fig. 10. Operation has been pushed to 37,000 fps in air at an initial pressure of 50μ Hg with a test time of 2-3μ sec. At lower shock speeds and higher pressures the test time is correspondingly longer. This shock tube is similar to a conventional combustion-driven tube, but up to 60,000 joules are discharged into the driver section, which is shown schematically in Fig. 11. The shock tube is of 6 in. inside diameter and the driver 1.5 inches. The driver is fitted with a teflon insulator tube, and is filled with helium at 300 psi prior to discharge.

Figure 12 shows a photomultiplier measurement of the radiation in the 5000A - 10,000A wavelength region behind a normal shock at 33,000 fps in air at an initial pressure of 0.1 mm Hg.

The oscillogram shows the radiation overshoot and then decay to an equilibrium level. A time-resolved drum camera picture for the same operating conditions is shown in Fig. 13. The photograph shows the full width of the shock tube but is severely distorted in the axial direction. The luminous front on the left is followed by the darker equilibrium region, and then by the driver gas. The test slug is approximately 7 cm in length, or almost half the width of the shock tube.

2. Experimental Results

Some measurements of the integrated luminous front in air are shown as a function of the reciprocal of shock velocity in Fig. 14. Most of these values were published in Ref. 4, but recent measurements at pressures of 0.3 and 0.1 mm Hg in the electric shock tube are added. These measurements cover a small wavelength region near 3900A. The radiation from this portion of the $N_2^+(1-)$ band system has been observed to have greater intensity than that from any other wavelength region between 3600A (the pyrex cutoff) and 10,000A.

Similar measurements covering the range of the $N_2(1+)$ system are shown in Fig. 15. The integration of the radiation profile is carried out to a distance behind the shock at which the intensity level is 10% higher than the equilibrium level. Current experimentation is directed toward reducing the scatter of these data, by mounting the windows in flat plates which have sharp leading edges and which protrude well into the shock tube. This permits the measurement of radiation from a clean gas sample free from boundary layer effects.

Taken together, these two groups of measurements covering different wavelength regions can lead to some rough estimates of the integrated luminous front intensity. At 35,000 fps the contribution over the 0.5μ - 1μ wavelength region, mostly from the $N_2(1+)$ band system, is about 1 w/cm^2-steradian, or 6 w/cm^2 radiation toward the stagnation point. In addition, a contribution of roughly similar magnitude is to be expected from the $N_2^+(1-)$ system. One thus arrives at a lower limit $\approx$ 12 w/cm^2 toward the stagnation point. Similar arguments can lead to an upper bound estimate of the integrated radiation over the wavelength region 0.36μ - 1μ. At 35,000 fps, the measurements of Fig. 14 show a maximum integrated intensity of $\sim$10 w/cm^2- μ-steradian (at the brightest portion of the spectrum). By assuming a uniform spectral distribution over the interval of 0.64μ, one may infer a maximum radiative flux of $\sim$6.4 w/cm^2-steradian or $\sim$40 w/cm^2 toward the stagnation point. Here it is necessary to stress that this estimate is for a very limited spectral coverage, and that is does not include contributions

from the i.r. beyond 1μ or from the u.v. below 0.36μ.

Although the integrated luminous front radiation is the most important experimental observable, other information is obtainable from the experiments. The thickness of the nonequilibrium region behind a normal shock front is of particular importance for flight applications, since it governs the relative magnitudes of the equilibrium and nonequilibrium radiative heating at the stagnation point. When the ambient density is sufficiently high, the thickness of the nonequilibrium region will be small compared with the shock standoff distance and most of the gas cap will be in thermodynamic equilibrium. As the density is reduced, the luminous front thickness increases and the equilibrium gas cap becomes thinner. At sufficiently low density the equilibrium region vanishes and at still lower densities the luminous front becomes truncated. However, shock tube measurements behind normal shocks will yield complete radiation profiles as long as there is sufficient test time available. The time for the luminous front intensity to fall to a level 10% above equilibrium can be used as an effective measure of the nonequilibrium distance. For time measured in the laboratory coordinate system, $d_{0.1} = U_s t_{0.1}$. Values of $t_{0.1}$ are plotted vs. shock speed in Fig. 16. Measurements made at different initial pressures are presented on a single plot whose ordinate is the product $P_1 t_{0.1}$, which would be approximately independent of P_1 in a binary regime. Over the relatively small range of P_1 used in these experiments, a single curve can be drawn through the data points. By means of this curve, values of P_1 vs. $d_{0.1}$ are plotted in Fig. 17 for various values of shock speed. The region covered by experiment is indicated on the graph. It should be recognized that Fig. 16 presents an empirical curve which may not be valid at pressures significantly different from those used in the experiments. Nevertheless, Fig. 17 provides useful information for estimating the onset of truncation in flight and ballistic range applications.

Full understanding of the luminous front phenomena calls for much theoretical work, and for correlations between theory and experiment. Rate constants have been deduced from the exponential decay of the luminous front intensity (Ref. 22). The location of the radiation peak with respect to the shock front is also important for correlation purposes. Figure 18 shows some measurements of the time to peak intensity behind shock waves in pure nitrogen. As in Fig. 16, measurements made at different values of P_1 are presented on a single plot whose ordinate is the product of P_1 and time to peak. This should be independent of initial pressure in a binary regime. Also shown is a plot of the calculated time required for equilibration of the vibrational degrees of freedom of the nitrogen molecules. The

close correlation suggests that there may be some coupling between the electronic temperature T_e and the vibration temperature of the molecules. There are other indications, notably in the work of Gaydon and his co-workers (Refs. 25 and 26) that such a coupling exists. Present theoretical work at the Avco-Everett Research Laboratory is directed along these lines, but there are many problems in the determination of the appropriate vibrational temperature in a complex gas such as air.

DISCUSSION

Figure 19 shows the equilibrium radiative flux and the laminar aerodynamic heat transfer rate to a body with a 10 ft nose radius flying at 35,000 fps. The general formats and derivations of the curves shown on this figure are identical with those discussed in the second section of this paper. It is evident that the radiative heating is severe for values of $\rho/\rho_o \gtrsim 10^{-4}$. It is thus of great interest to determine the level of radiative heating due to the luminous front. At present there is insufficient experimental evidence to determine the location of the "luminous front plateau" on Fig. 19. The measurements quoted in the previous section for the limited spectral coverage of the $N_2(1+)$ and the $N_2^+(1-)$ systems set an approximate lower limit of 10 w/cm^2 for the integrated luminous front radiation, but contributions from other band systems and particularly from the far u.v. could conceivably produce an integrated radiation in excess of 100 w/cm^2.

When more experimental data are available, a reliable theory or mathematical model which correlates with the experiments would facilitate calculation of luminous front radiation for flight conditions not readily simulated in the laboratory. A satisfactory model for shock speeds in the neighborhood of 40,000 fps would involve estimation of the behavior of air at translational temperatures as high as 75,000 K. The present uncertainties in such a model include:

1) The method of extrapolation of rate constant information to such high temperatures.

2) The behavior of the various vibrational and electronic temperatures behind the shock wave, and their interrelationships.

3) The coupling between the vibration and dissociation processes, and its effect on the reduction of translational temperature.

4) Rate constant information for ionization reactions involving collisions between electrons and neutrals.

5) Knowledge of the excitation mechanisms and cross sections for the various band systems.

The problem clearly offers almost unlimited scope for theory and experiment, and is potentially very important with respect to the re-entry and recovery of satellites launched into highly elliptical orbits.

ACKNOWLEDGMENT

The authors wish to acknowledge the advice and assistance given by their colleagues at Avco-Everett Research Laboratory. They also acknowledge many fruitful discussions with NASA personnel at Ames Research Center.

REFERENCES

1 Fay, J.A. and Riddell, F.R., J. Aero. Sci., vol. 25, 1958, p. 73.

2 Rose, P.H. and Stark, W.I., J. Aero. Sci., vol. 25, 1958, p. 86.

3 Kivel, B., J. Aero/Space Sci., vol. 28, 1961, p. 96.

4 Meyerott, R.E., Lockheed Aircraft Corp. Missile Systems Division, Palo Alto, Calif., LMSD-2264, Nov. 1957.

5 Camm, J., Kivel, B., Taylor, R. and Teare, J.D., Avco-Everett Research Lab., Research Rep. 93, Dec. 1959; also J. Quantitative Spectroscopy Radiative Transfer, vol. 1, 1961, p. 53.

6 Duff, R.E. and Davidson, N., Bull. Am. Phys. Soc. II, vol. 4, 1959, p. 195; also J. Chem. Phys., vol. 31, 1959, p. 1018.

7 Lin, S.C. and Teare J.D., Bull. Am. Phys. Soc. II, vol. 4, 1959, p. 195.

8 Wray, K.L. and Teare, J.D., Avco-Everett Research Lab., Research Rep. 95, Aug. 1961. (To be published)

9 Wray, K.L. Teare, J.D., Kivel, B. and Hammerling P., Avco-Everett Research Lab., Research Rep. 83, Dec. 1959; also Proc. 8th Symposium (International) on Combustion, Pasadena, Calif., 1960.

10 Wray, K.L., ARS Preprint no. 1975-61, Aug. 1961.

11 Kennet, H. and Strack, S.L., ARS J., vol. 31, 1961, p. 370.

12 Goulard, R., J. Aero/Space Sci., vol. 28, 1961, p. 158.

13 Adams, M.C. and Probstein, R.F., Jet Propulsion, vol. 28, 1958, p. 86.

14 Kivel, B. and Bailey, K., Avco-Everett Research Lab., Research Rep. 21, Dec. 1957.

15 Keck, J.C., Camm, J.C., Kivel, B. and Wentink, T.,Jr., Annals of Physics, vol. 7, 1959, p. 1.

16 Allen, R.A., Camm, J.C. and Keck, J.C., Avco-Everett Research Lab., Research Rep. 102, April, 1961. (To be published in J. Quantitative Spectroscopy Radiative Transfer, Nov. 1961).

17 Wurster, W.H. and Marrone, P.V., CAL Rep. no. QM-1373-A-4, Cornell Aeronautical Lab., Buffalo, N.Y., July, 1961.

18 Treanor, C.E., published elsewhere in this volume.

19 Keck, J., Camm. J. and Kivel, B., J. Chem. Phys., vol. 28, 1958, p. 723.

20 Hammerling, P., Teare, J.D. and Kivel, B., Proc. 4th International Conference on Ionization Phenomena in Gases, (Uppsala, Sweden, Aug. 1959), North-Holland Publishing Co., 1960.

21 Hammerling, P., Teare, J.D., Kivel, B., Phys. Fluids, vol. 2, 1959, p. 422.

22 Allen, R.A., Camm, J.C., and Keck, J.C., Avco-Everett Research Lab., Research Rep. 110, June 1961.

23 Lin, S.C. and Fyfe, W.I., Phys. Fluids, vol. 4, 1961, p. 238.

24 Rosa, R.J., Phys. Rev., vol. 99, 1955, p. 633.

25 Clouston, J.G., Gaydon, A.G. and Hurle, I.R., Proc. Roy. Soc., A, vol. 252, 1959, p. 143.

26 Gaydon, A.G. and Hurle, I.R., Proc. 8th Symposium (International) on Combustion, Pasadena, Calif., 1960.

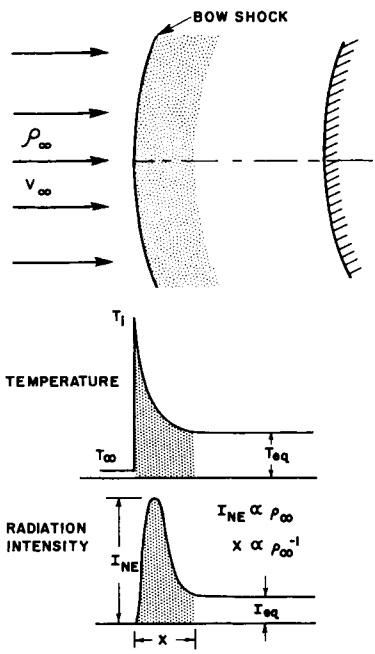

Fig. 1 Schematic diagram of the nonequilibrium region behind the bow shock at the stagnation point of a blunt body.

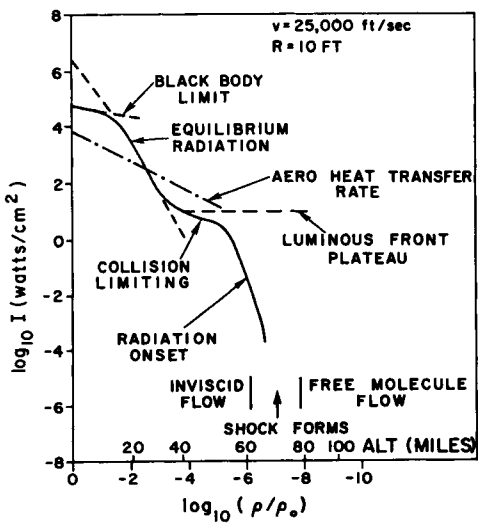

Fig. 2 Comparison of radiative and aerodynamic heat transfer as a function of ambient density for flight speed of 25,000 fps and nose radius R = 10 ft.

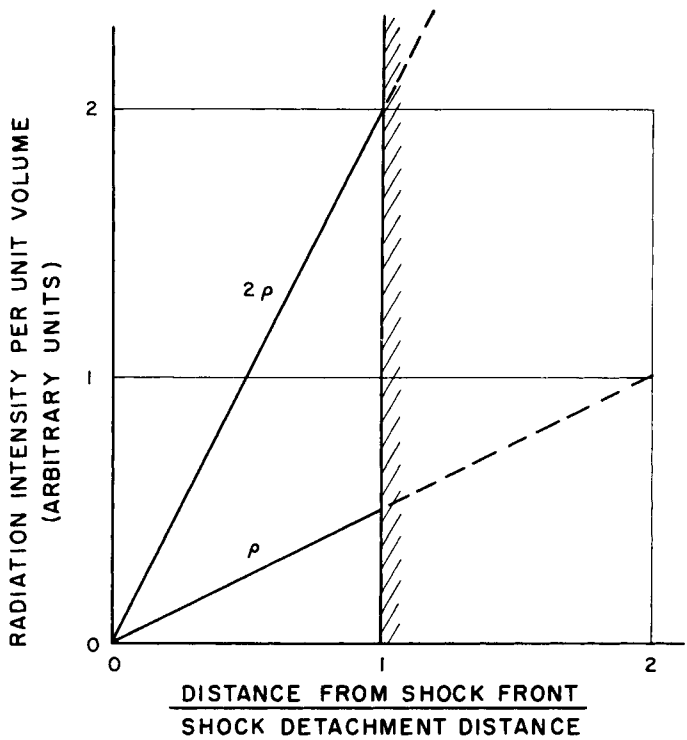

Fig. 3 Schematic diagram of luminous front truncation for a linear rise of radiation intensity. A factor of 2 increase in ambient density results in a fourfold increase in radiation intensity at a given distance behind the shock front, leading to a ρ^2 dependence for the integrated intensity behind a truncated shock front.

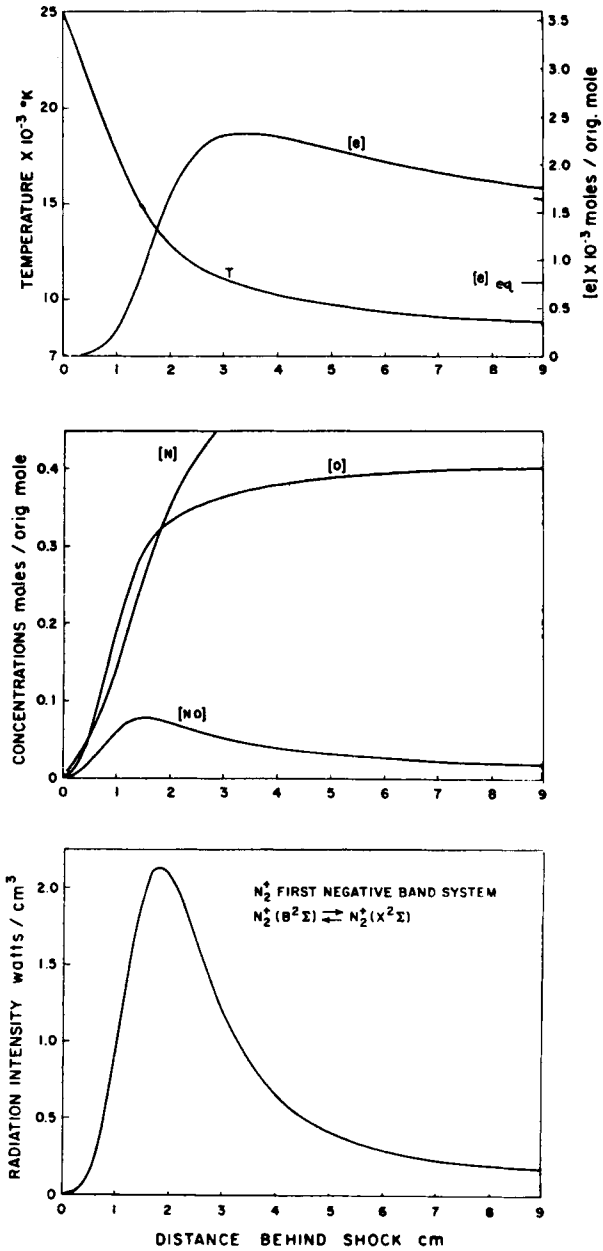

Fig. 4 Relaxation behind a shock wave travelling at 23,500 fps into air at an initial pressure of 20μ Hg. Concentrations are expressed in moles per mole of unshocked gas. This figure is reproduced from Ref. 5. In view of the revised f number quoted (Ref. 16) for the $N_2^+(1-)$ band system, the plotted intensity levels should be reduced by a factor of 2.

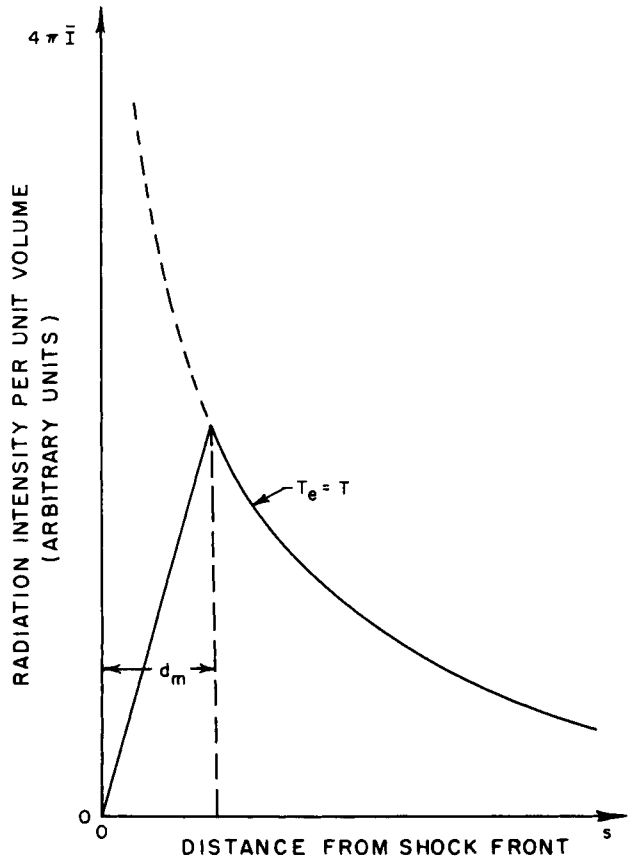

Fig. 5 Schematic diagram of radiation profile. For $s \geq d_m$, it is assumed that $T_e = T$. For $s < d_m$, $\bar{I}$ increases linearly with s.

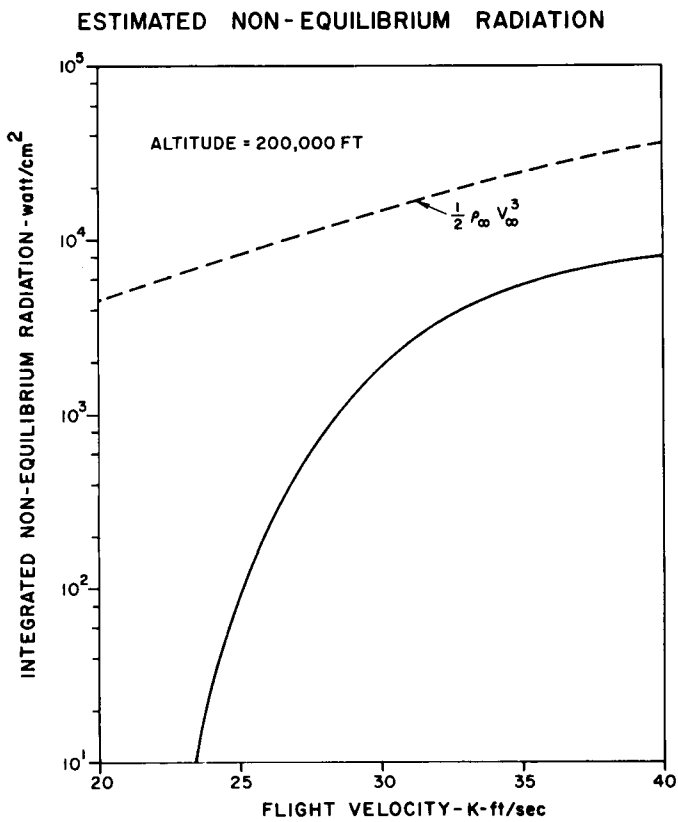

Fig. 6 Preliminary estimate of the integrated nonequilibrium radiation as a function of flight velocity at 200,000 ft altitude. The solid curve shows the results of calculations based on a very tentative model of the relaxation region. It is presented purely to stress the need for experimental measurements in this velocity range. The broken curve shows the incident energy flux per unit area of bow shock.

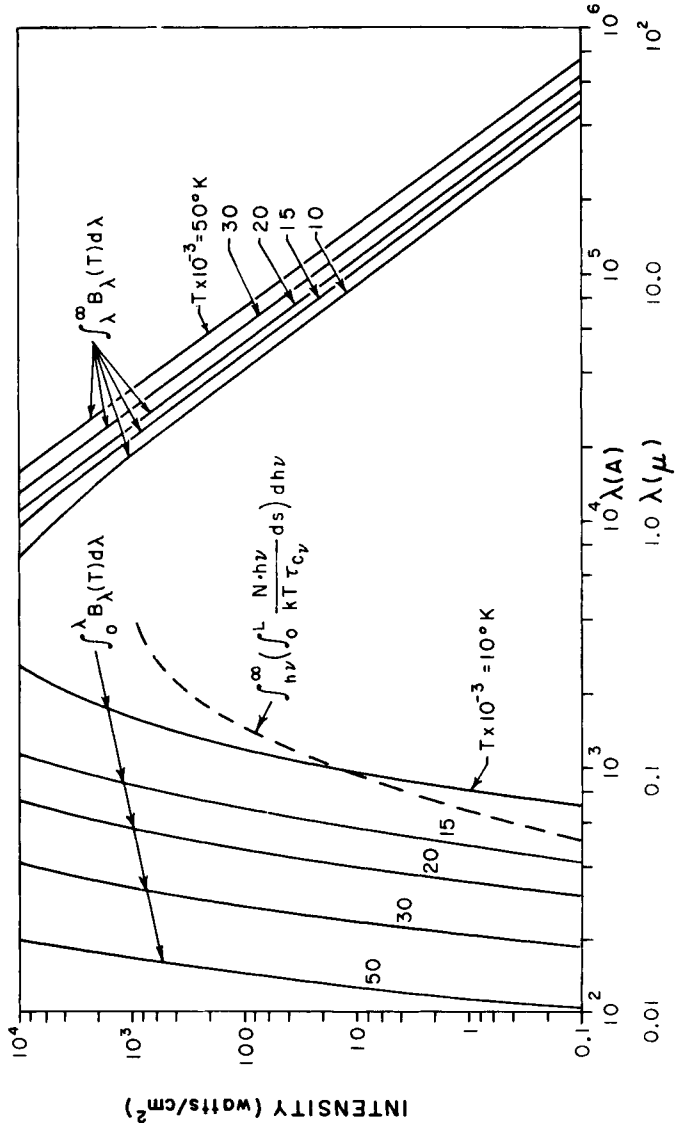

Fig. 7 Integrated Planck intensities from the i.r. and the u.v. for several temperatures. Also shown is an upper-bound estimate of the radiation from the relaxation region shown in Fig. 4, based on an excitation cross section of 10^{-15} cm^2 according to Eq. 7 in text.

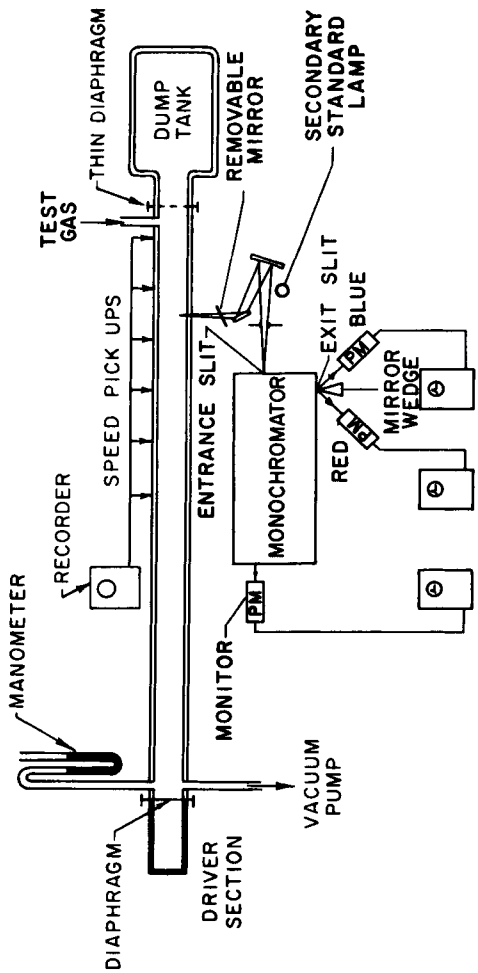

Fig. 8 Schematic diagram of 1.5 in. combustion-driven shock tube. The removable mirror and secondary standard lamp are used in the calibration procedure.

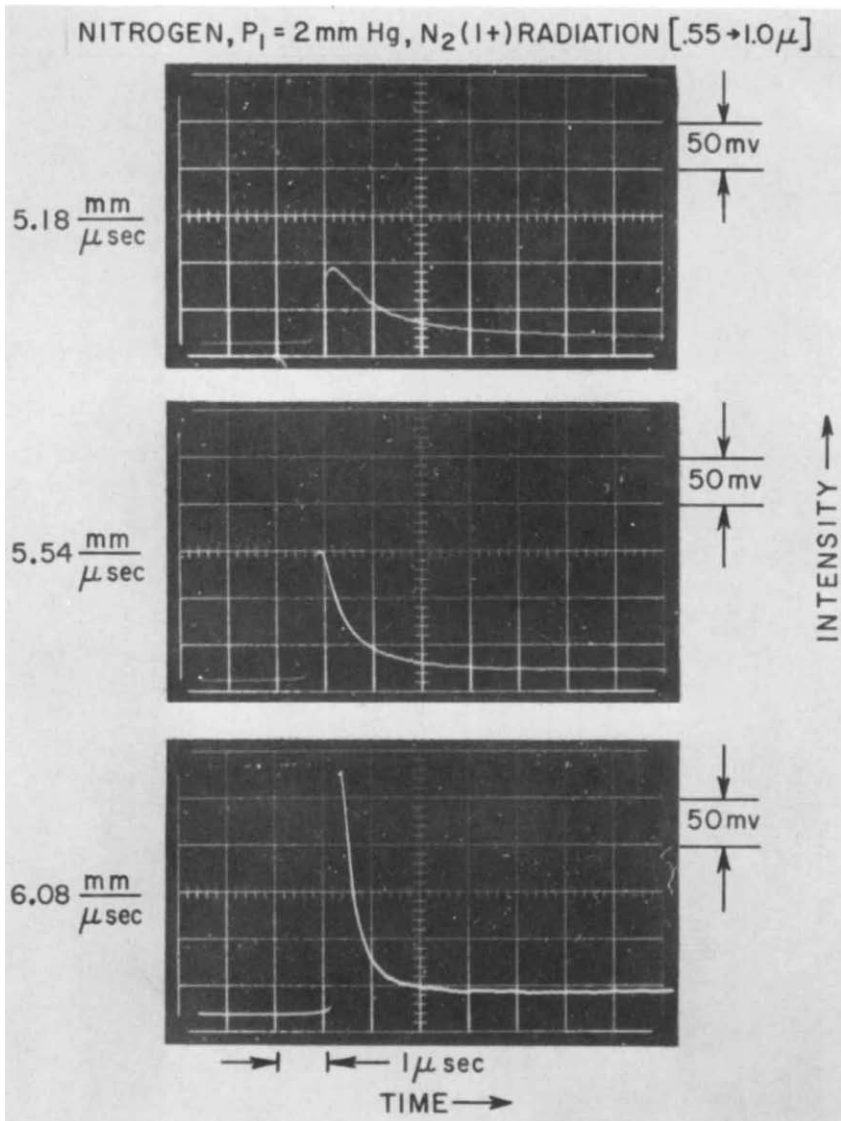

Fig. 9 Typical oscillograms of the nitrogen first positive band system radiation from shock waves in pure N_2 showing the radiation overshoot behind the shock front and subsequent relaxation to equilibrium for several shock speeds.

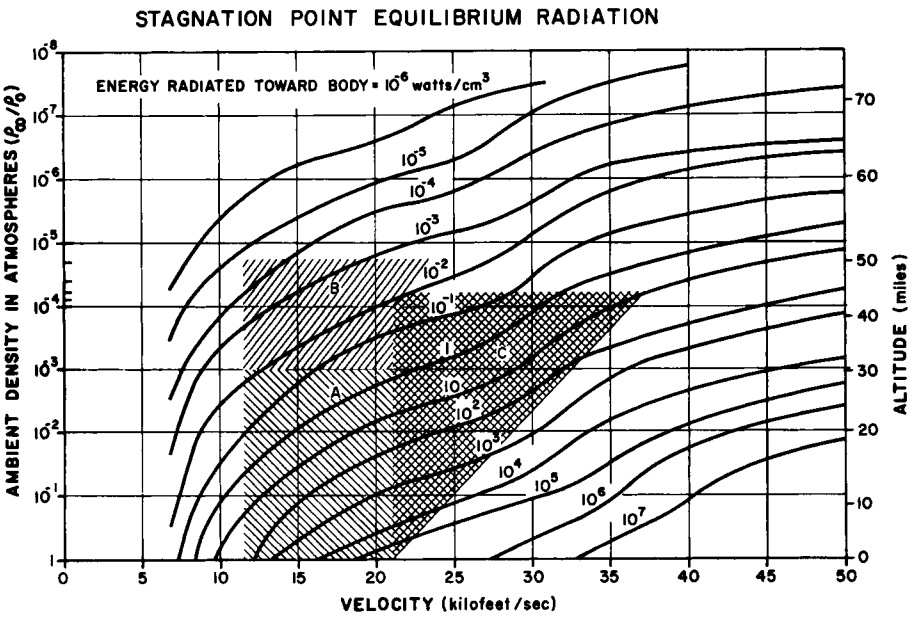

Fig. 10 Approximate operating regions for shock tube radiation measurements in terms of shock velocity and ambient air density.

A) Conventional combustion-driven shock tubes.
B) 24-in. low density shock tube.
C) Electrically driven shock tube.

The contours show one-half $(2\pi\bar{I})$ of the emitted radiation energy per unit volume from the stagnation region for fully equilibrated air. For an optically thin gas, this represents an energy flux towards the stagnation point in w/cm^2 per unit thickness of gas cap.

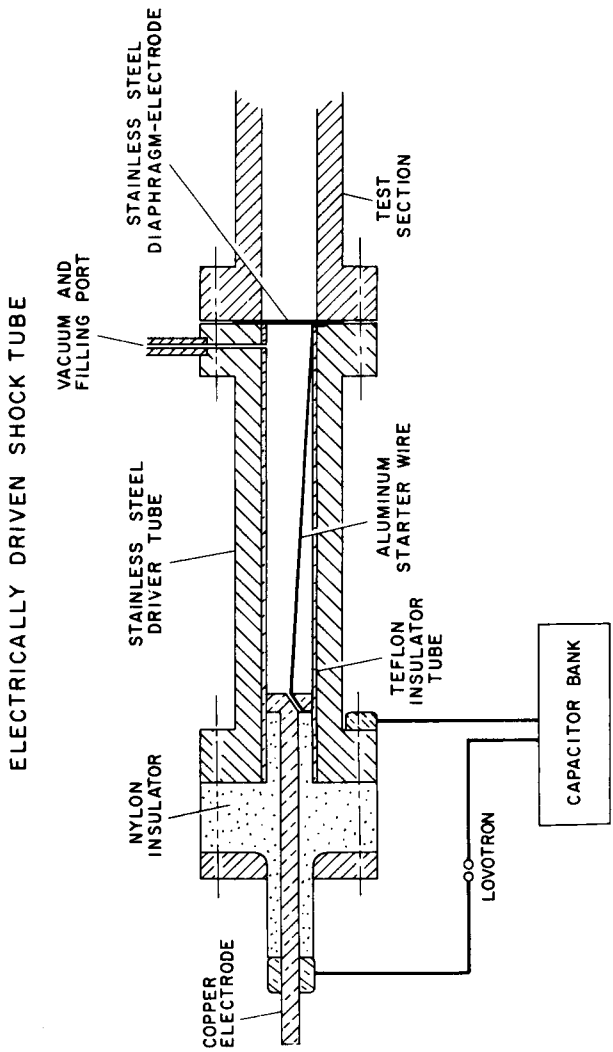

Fig. 11 Schematic diagram of driver section for electric shock tube.

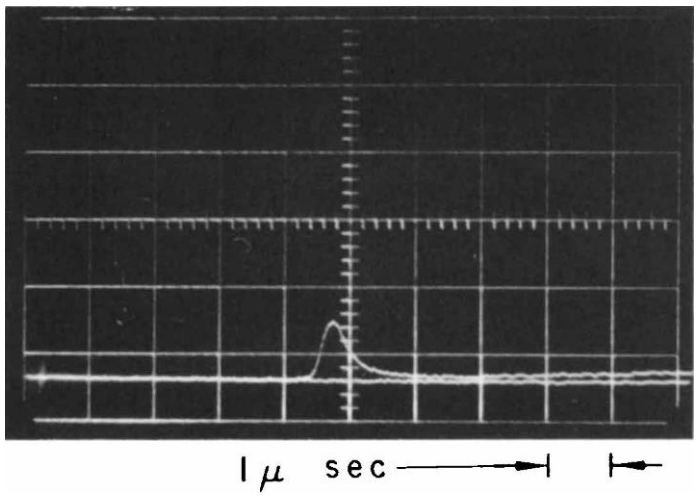

Fig. 12 Oscillogram of the nitrogen first positive radiation behind a normal shock in air in the electric shock tube. The wavelength region is 5000A - 10,000A, U_s = 33,000 fps, P_1 = 0.1 mm Hg.

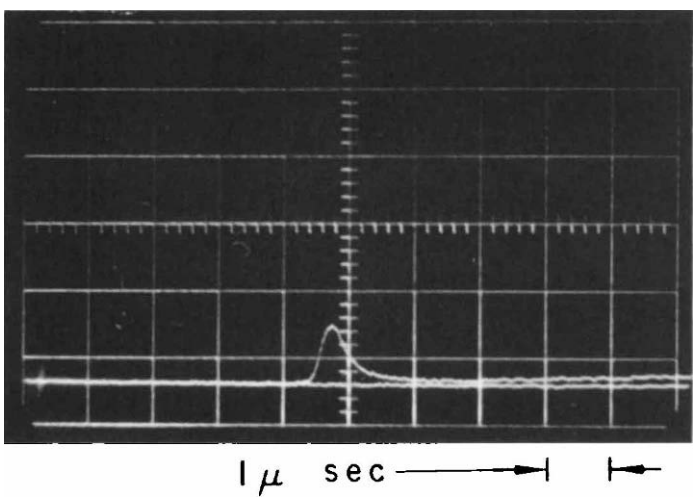

Fig. 13 Time resolved drum camera photograph of normal shock in air in electric shock tube, showing luminous front radiation at left, followed by equilibrium region and driver gas. U_s = 33,000 fps, P_1 = 0.1 mm Hg. The photograph shows the full width of the shock tube, but is distorted in the axial direction. The test slug is approximately 7 cm in length.

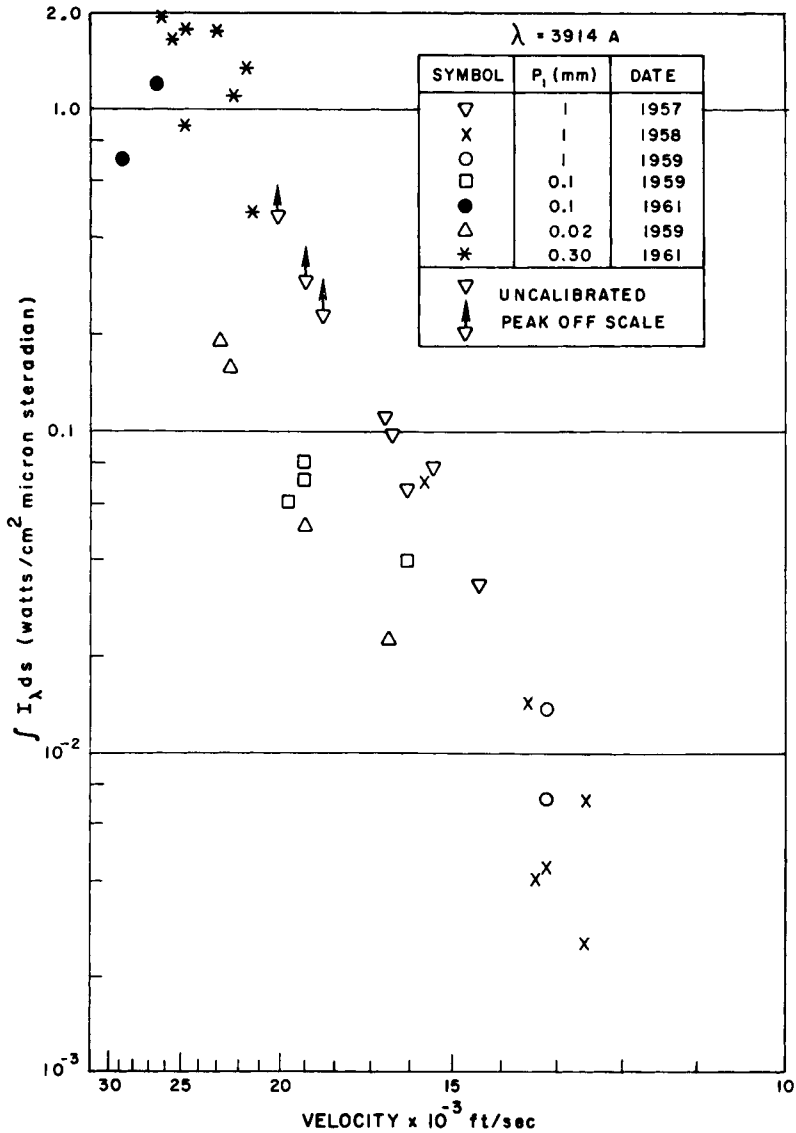

Fig. 14 Integrated luminous front intensity for λ = 3914A in air as a function of the reciprocal of the shock speed. This radiation is due to the $N_2^+(1-)$ band system. The measurements cover a bandwidth of 200A. Note that the units of the ordinate scale differ from those of Fig. 15.

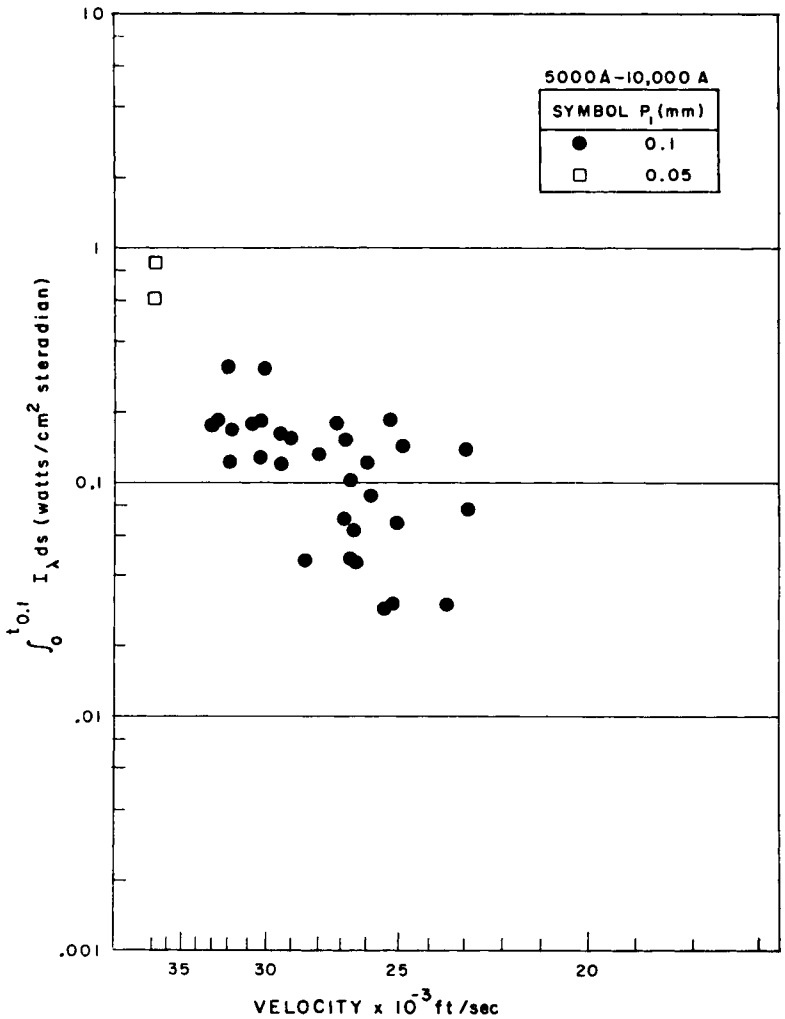

Fig. 15 Integrated luminous front intensity for the $N_2(1+)$ band system in air as a function of the reciprocal of the shock speed. The integration is carried out to a distance behind the shock front at which the radiation intensity is 10% higher than the equilibrium level.

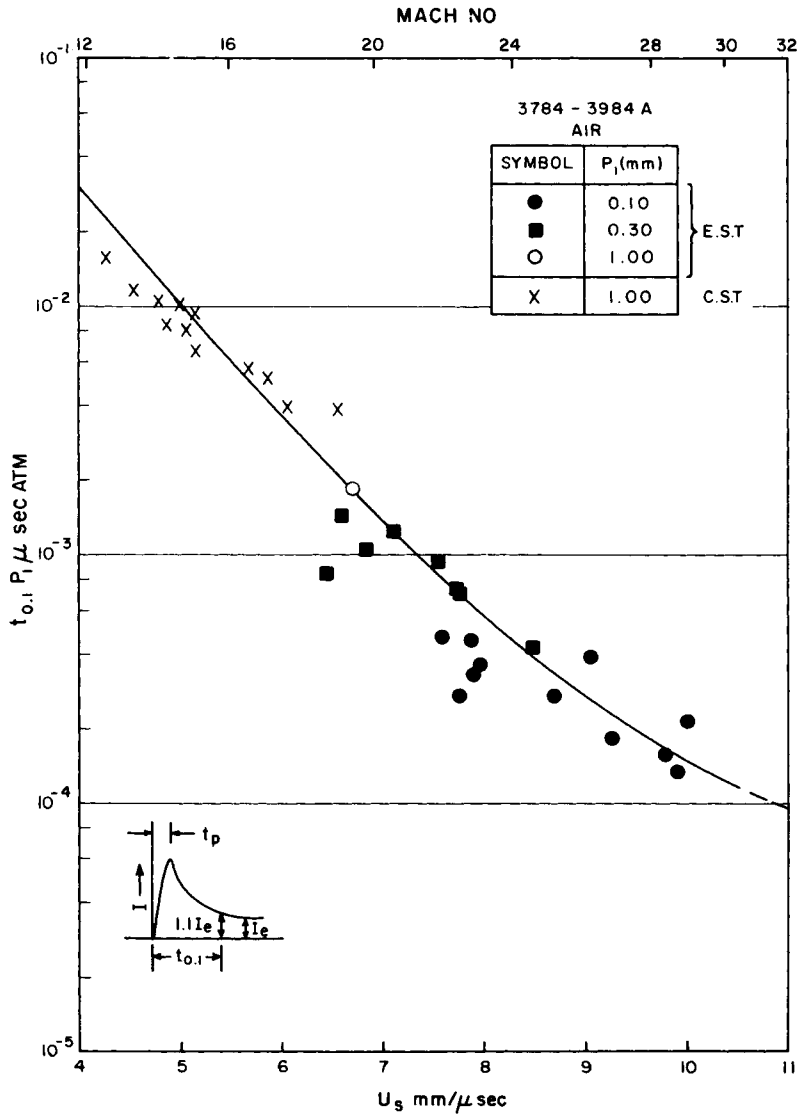

Fig. 16 Observed time duration of luminous front in air, plotted versus shock speed. The time $t_{0.1}$ in the laboratory coordinate system is taken to a point at which the radiation intensity has decayed to a level 10% above equilibrium. Initial pressure is used as a scaling factor to correlate data obtained at different values of P_1 . The solid line is an empirical curve drawn through the data.

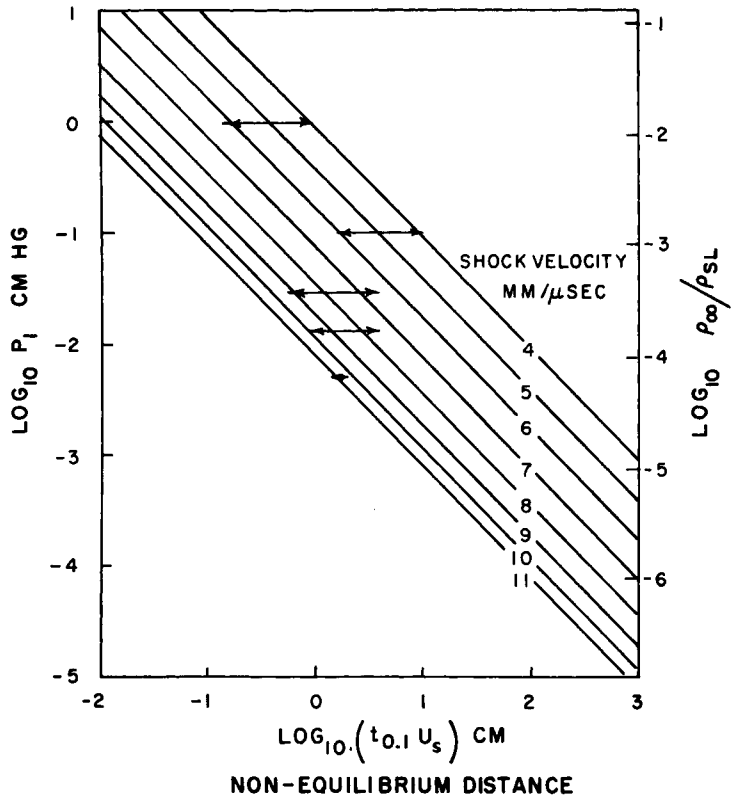

Fig. 17 Initial pressure P_1 is plotted against luminous front thickness $d_{0.1}$ for various shock speeds. In the laboratory coordinate system $d_{0.1} = U_s t_{0.1}$. The lines have been constructed by means of the empirical curve of Fig. 16. Arrows indicate the regions covered by the experiment.

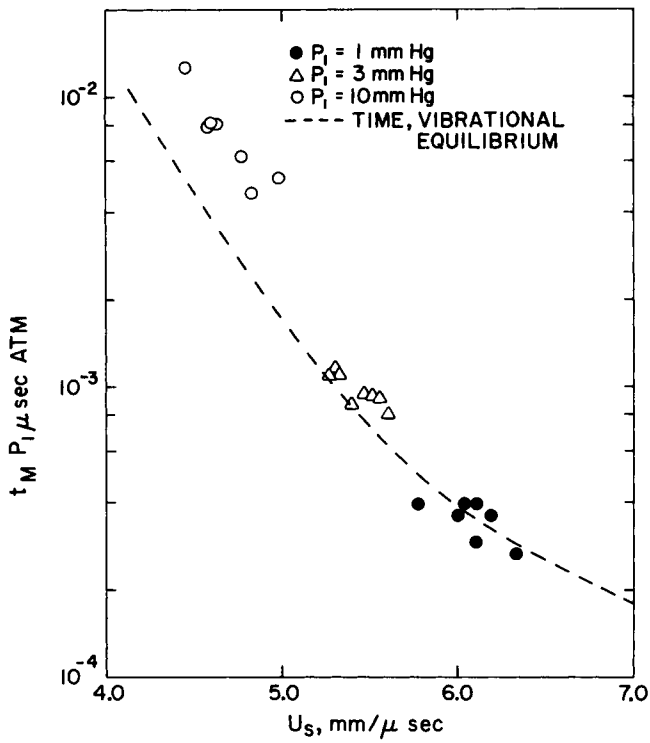

Fig. 18 Observed time of peak radiation t_M for the $N_2(1+)$ system in pure nitrogen, plotted vs. shock speed. Initial pressure is used as a scaling factor to correlate data obtained at different values of P_1 . The calculated time for equilibration of the vibrational degrees of freedom of the molecules is also shown.

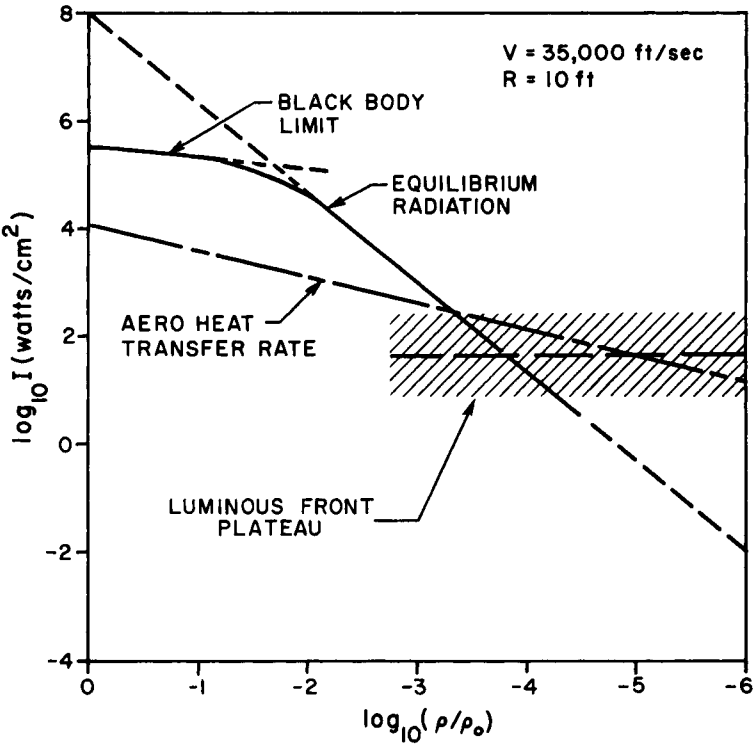

Fig. 19 Comparison of radiative and aerodynamic heat transfer as a function of ambient density for a flight speed of 35,000 fps and nose radius R=10 ft. The location of the luminous front plateau is not yet known. The lower limit shown is based on the measurements of Figs. 14 and 15.